Micromagnetic understanding of evolutions of antiferromagnetic domains in NiO

Magnetic materials generally form magnetic domains to reduce the total energy of the system [1]. While magnetic domains in ferromagnets have been extensively studied for both fundamental and technological importance, those in antiferromagnets have not been investigated as much. In the recently emerging antiferromagnetic spintronics [2], antiferromagnetic domain formations and its dynamics are becoming implicit questions and are key to elucidate the antiferromagnetic behaviors in response to various extraneous fields such as magnetic field, spin orbit torque [3], and electric field. Since antiferromagnets do not have spontaneous magnetization, the magnetocrystalline anisotropy and magnetoelastic energies often dominate over the negligible magnetostatic energy, which bring about the domain formations and evolutions in completely different manner than those of ferromagnets. Therefore, one often experiences a difficulty to simulate antiferromagnets with conventional micromagnetic simulation packages (e.g., OOMMF, mumax^3, etc.) primarily designed for ferromagnets.

In this study, we experimentally investigate formations and evolutions of antiferromagnetic domains in NiO (001) of a bulk single crystal, which is an archetypical collinear antiferromagnet, with a strong external magnetic field. By implementing the crystallographic continuity into the magnetic energy calculations, we then establish a unique micromagnetic simulation algorithm for the antiferromagnetic NiO and understand the domain formations and evolutions.

NiO shows a rock-salt structure above the Néel temperature T_N = 523 K and it sustains a slight rhombohedral distortion in one of the <111> directions below T_N. In the antiferromagnetic phase, there are two different magnetic anisotropies due to the crystalline symmetry. One is a strong magnetic *easy-plane* anisotropy lying on a {111} plane which is strongly coupled with the rhombohedral distortion and promotes the so-called *T*-domain (Fig. 1). The other is a weak three-fold *in-plane* anisotropy in the <11$\bar{2}$> directions in the {111} plane which promotes the so-called *S*-domain. Therefore, one *T*-domain always contains a few of the three *S*-domain. Combination of these magnetic anisotropies results in 12 different orientations of Néel vectors in *T*- and *S*-domain. Here, we label a *T*-domain associated with (111) as T_1 and *S*-domain with [$\bar{2}$11] as **S$_1$** and so on as indicated in Fig. 1.

Since *T*-domain always associates with the rhombohedral distortion, crystallographic continuity is the most important consideration to construct the micromagnetic structure. Considering the rhombohedral symmetry, the boundaries in the same symmetry are classified by colors for each *T*-domain unit-cell as shown in Fig. 1. With this classification, connection between *T*-domain unit-cells is preferentially made with the same color boundary.

For the micromagnetic simulations, we consider the four different potential energies involved for the stabilization of the ground state which are associated with (1) the *boundary connections* (U_B), (2) the *T-domain connections* (U_T), (3) the *S-domain connections* (U_S), and (4) the *Zeeman energy* (U_Z). The *boundary connections* consider increase of the potential energy if a connection between different color boundaries is made. For the *T-domain connections*, the potential energy increases when neighboring *T*-domains are discrepant. Similarly, for the *S-domain connections*, the potential energy increases when neighboring *S*-domains are discrepant. The *Zeeman energy* characterizes the Néel vector orientation with respect to the external magnetic field.

Figure 2 shows the X-ray magnetic linear dichroism photoemission electron microscopy (XMLD-PEEM) images and the ones constructed by the micromagnetic simulation of a virgin (001) surface of a cleaved NiO before applying external magnetic field. The XMLD-PEEM images were taken by *p*-polarized X-ray beam incident with photon energies at the oxygen *K*-edge and the Ni L_2-edge at SPring-8 **BL17SU**. Figures 2(a) and 2(c) essentially reflect the *T*-domain and *S*-domain patterns, respectively. The pattern with the O *K*-edge is found to be very sharp and shows only one contrast. On the other hand, the pattern with Ni L_2-edge is more complex with more than two contrasts. We first construct the *T*-domain pattern by minimizing $\Sigma_x^n \Sigma_y^n \Sigma_{t=0}^1 U_B$ and reproduce the one experimentally obtained. As one can see in Fig. 2(b), the reproduced *T*-domain pattern

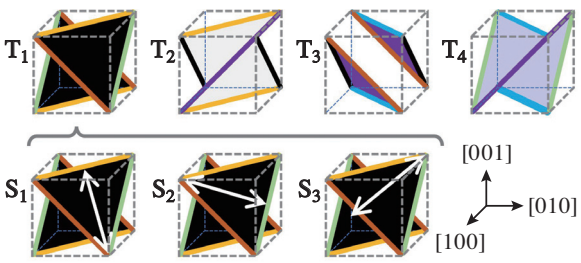

Fig. 1. Easy-plane orientations of *T*-domains and the easy axes of the *S*-domains.

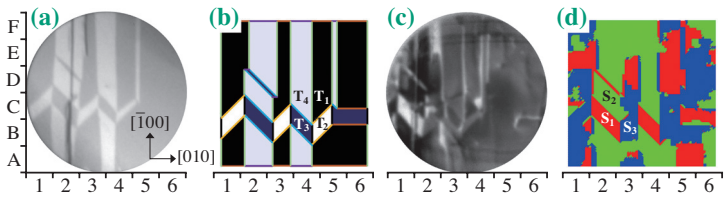

Fig. 2. XMLD-PEEM images taken with the photon energy at the O *K*-edge **(a)** and Ni L_2-edge **(c)** which respectively represent *T*-domain and *S*-domain patterns. The reproduced *T*-domain **(b)** and *S*-domain pattern **(d)** by the micromagnetic simulation.

has no discrepancies on the boundary connections. Most importantly, it almost completely reproduces the detailed domain structures seen in Fig. 2(a). One can see even the small details in the locations: C-5, D-3, and E-2 in Fig. 2(a) are perfectly reproduced. The contrast with Ni L_2-edge is more complex and does not directly accord with the simulated *S*-domain pattern (Figs. 2(c) and 2(d)). For the meanwhile, we start from these initial *T*- and *S*-domain patterns and investigate antiferromagnetic domain evolutions after applying external magnetic fields.

Starting from the initial state shown in Fig. 2, we take XMLD-PEEM images after a magnetic field application and analyze them with the corresponding *T*-domain and *S*-domain patterns reproduced by the simulation. The results are displayed in Fig. 3.

The *T*-domain patterns observed by the O *K*-edge are almost kept the same after the field is applied in either [010] or [100] direction (Figs. 3(a-c)). The simulations reproduce the pattern very well (Figs. 3(f-h)) which are essentially unchanged under the magnetic fields. The experimental observations and the simulation results can be explained by the *Zeeman energy* term U_Z. The system can minimize U_{tot} by switching *S*-domain without changing *T*-domains, leading to the invariant *T*-domain pattern. The same arguments apply to the [100] field.

Remarkable changes in the domain patterns are observed when the magnetic field is applied in [$\bar{1}$10] and [$\bar{1}\bar{1}$0] directions. As seen in Fig. 3(d), the change in the *T*-domain pattern taken after the [$\bar{1}$10] field application is quite dramatic. The longitudinal domains disappear, and the diagonal domains expand along the field direction, which are perfectly reproduced by the simulation (Fig. 3(i)).

In summary, we experimentally investigate and numerically simulate evolutions of antiferromagnetic domains in a cleaved NiO (001) under magnetic fields. First, we clearly observed, by the XMLD-PEEM, the antiferromagnetic domain evolutions with a strong magnetic field and its behavior strongly depending on the magnetic field direction. Second, by considering the appropriate potential energy factors taking into account the crystallographic symmetry as well as relevant magnetic energies, we established a unique micromagnetic simulation algorithm to reproduce details of the experimentally observed antiferromagnetic domain evolutions [4].

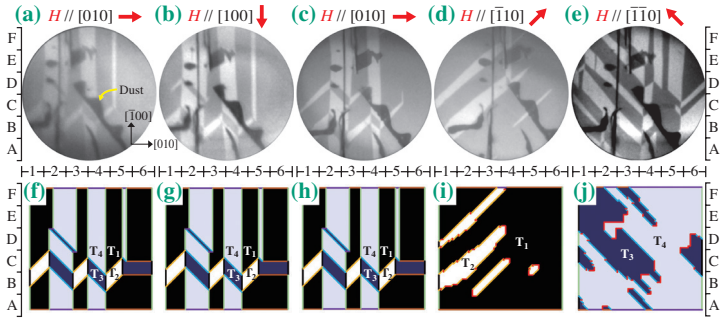

Fig. 3. **(a-e)** XMLD-PEEM images taken with the photon energy at the O *K*-edge after each magnetic field application. **(f-j)** Corresponding *T*-domain patterns reproduced by the simulations. The red boundaries indicate the discrepancy boundary connection, i.e., connection between different color boundaries. The alphabet-number coordinate system is referenced to specify a location.

Takahiro Moriyama

Department of Materials Physics, Nagoya University

Email: moriyama.takahiro.a4@f.mail.nagoya-u.ac.jp

References

[1] S. Chikazumi: Physics of Ferromagnetism (OUP Oxford, New York, 2009).
[2] V. Baltz *et al.*: Rev. Mod. Phys. **90** (2018) 015005.
[3] T. Moriyama *et al.*: Sci. Rep. **8** (2018) 14167.
[4] *T. Moriyama, L. Sánchez-Tejerina, K. Oda, T. Ohkochi, M. Kimata, Y. Shiota, H. Nojiri, G. Finocchio and T. Ono: Phys. Rev. Mater. 7 (2023) 054401.*